

HYDRAULIC ACTUATOR LEAKAGE FAULT DETECTION USING EXTENDED KALMAN FILTER

Liang An and Nariman Sepehri

Department of Mechanical and Manufacturing Engineering, The University of Manitoba, Winnipeg, MB, Canada R3T 5V6
umanl@cc.umanitoba.ca, nariman@cc.umanitoba.ca

Abstract

This paper presents the application of extended Kalman filter (EKF) in order to identify leakage faults in hydraulically powered actuators. A hydraulic actuator can suffer from two types of leakages: internal or cross-port leakage at the piston seal and, external leakage at the shaft seal or the connecting pipes. An EKF-based estimator is constructed that includes complete nonlinear models of hydraulic functions as well as inevitable stick-slip friction in the actuator. It is shown that, firstly, under normal (no-fault) operating condition, the developed estimator closely predicts the states of the system, using only a few basic measurements. Secondly, in the presence of leakage faults, the level of residual errors between the estimated and the measured line pressures, increase significantly indicating the occurrence of faults. Thirdly, different leakage types can be identified by mapping the residual errors changes. Experiments are performed on a laboratory-based hydraulic actuator circuit. The results demonstrate the efficacy of the proposed EKF-based fault detection scheme to promptly and reliably respond to actuator's external and internal leakage faults.

Keywords: fault detection and isolation, extended Kalman filter, leakage, hydraulic actuators.

1 Introduction

Fluid power systems condition monitoring are earning more and more consideration to reduce the cost of maintenance and prevent the system fault from further deteriorating by detecting the fault in its incipient stage. One of the common faults associated with fluid power systems, is the leakage of hydraulic fluid from the fittings and lines that connect the components of the system together, or leaks across the seals that allow relative motion between mechanical components (Skormin et al, 1994). Leakage will cause inefficient performance in a hydraulic system. With the leakage deteriorating, the system will eventually break down. A sudden leakage could also trigger serious consequences when the system is working with load and is always a major threat to machine operators. Depending upon whether the hydraulic fluid is lost to the atmosphere or is dissipated to another location within the hydraulic circuit, leakage may be classified as external or internal, respectively.

The focus of this paper is on hydraulic actuator leakage fault detection. Two types of leakages were considered. The first type is internal (cross-port) leakage of fluid across the actuator piston seal that closes the gap between the moveable piston and the

cylinder wall. Although no fluid is lost from the circuit, the dynamic performance of the system is affected since portion of the flow delivered to the actuator is unable to push the piston against the load. The net effect of cross-port leakage is to increase the damping characteristic of the actuator as the degree of leakage increases (Karpenko and Sepehri, 2004). In the case where the piston seal fails completely, the actuator will lose the ability to effectively manipulate the load. Wear of the seals separating the actuator rods and the cylinder results in leakage of hydraulic fluid to the atmosphere. This type of external leakage results in a sluggish response. External leak could also be due to failure of a hydraulic supply line or connections between the valve and the actuator's chambers.

A great deal of work has been carried out on development of fault detection and isolation (FDI) systems in the past decade. A detailed survey on existing techniques has been summarized by Isermann (1997). As far as the application to the highly dynamic and nonlinear hydraulic systems is concerned, Skormin et al (1994; 1995) constructed a linear model for an electrohydrostatic flight actuation system in which leakage in the hydraulic pump, fault in the control valve, changes in the bulk modulus, and fault due to excessive friction were studied via only simulations. In their work, the

This manuscript was received on 25 August 2004 and was accepted after revision for publication on 5 February 2005

system's equations were linearized and represented by an autoregressive with exogenous inputs model. Using a similar parametric approach, Song and Sepehri (2002) successfully showed a possible way for detecting pump failure when the hydraulic system operates under periodic input signals. No leakage fault detection was considered in their paper. Alternatively, Tan and Sepehri (2002) applied the Volterra nonlinear modelling concept to implement an FDI scheme in hydraulic actuation systems. By constructing a parametric space, changes in the supply pressure or hydraulic compliance and actuator leakage faults were detected. However, systems with various faults must be emulated and Volterra models must be developed beforehand. This may not be feasible from the application view point.

Artificial neural networks (ANN) have also found their applications in the general area of FDI. Within the context of fluid power systems, Crowther et al (1998) presented an output vector space classification approach for incorrect pump pressure fault, increased load dynamic friction and cross-port leakage fault diagnosis in a hydraulic actuator. They showed that the internal leakage can be isolated from the other two faults. However, external leakage type was not considered in their research. Le et al (1998) detected and identified internal and external leakages for an electrohydraulic actuation system using a multi-layer perception ANN and, by working with only the pressure transient responses. The importance of their work was the ability to discriminate between different types of leakage faults especially when involving multiple leaks. However, several neural models, corresponding to various fault types and levels, needed to be trained based on data obtained from the system undergoing various leakage types and flow rates.

Fault detection schemes based on state-space analysis have also been under consideration, and various nonlinear observers have been developed for this purpose (see the survey by Frank, 1994 and the references therein). To name a few, Khan et al (2002) applied a nonlinear observer to detect incorrect supply pressure in a typical hydraulic actuator. The actuator velocity was the only measurement in their work. Yu et al (1994) developed a bilinear fault detection observer for a hydraulic motor-loading system to detect the pump shaft speed sensor fault as well as changes in the effective viscous coefficient. Based on only simulation results, they showed that the proposed scheme is effective in detecting these faults. No leakage fault was considered in their study. Built upon the work by Yu et al (1994), Preston et al (1996) simulated the performance of a nonlinear observer to detect changes in the spool valve displacement, pressure across the motor and motor angular speed. Isolation of the above faults, however, was shown to be difficult.

The application of Kalman filter (KF) in the field of FDI is relatively new. Being a computationally intense algorithm, KF has been widely applied only after the rapid development of high-speed low-cost computers (Haykin, 2001). As an important extension of KF, extended Kalman filter (EKF) linearizes the model of the nonlinear system about the latest estimates; thus, it can closely track the state trajectories for nonlinear sys-

tems. Khoshzaban et al (1999) showed the feasibility and advantage, over other existing techniques, of applying an EKF-based algorithm towards intelligent monitoring of a two-stage proportional flow control servovalve. An and Sepehri (2003) developed an EKF-based scheme capable of detecting the incorrect supply pressure fault and experimentally verified that the scheme could effectively detect a pressure change of less than 10% of the nominal value. Chinniah et al (2003) showed that the bulk modulus and the viscous damping coefficient of a hydrostatic actuation system could be correctly estimated, in sequence, using EKF. From the above papers, it is noted that a general approach for fault detection and isolation in nonlinear fluid power systems is complicated to develop. Also, the actuator leakage fault detection has not yet received enough attention. Karpenko and Sepehri (2004) developed a fault tolerant control scheme for a hydraulic servo-positioning system with a faulty actuator piston seal that causes internal leakage. They showed that implementing a fault tolerant control scheme allows the closed-loop performance to be maintained despite the internal leakage until the system can be safely shut down and the faulty seal replaced. Although its importance was discussed, the paper did not consider the identification of level and type of leakage.

In this paper, we develop and experimentally evaluate, for the first time to our knowledge, a scheme that employs EKF to identify various leakage type faults in an electrohydraulic actuator. External leakage from either side of the actuator, and cross-port leakage between the two chambers are considered. In the present work, these faults are assumed to occur singly, but exist in a multiple-fault environment. By comparing the actuator chamber pressures that are easy to measure with the corresponding estimates from the EKF model, information regarding the actuator leakage fault conditions is established. No model of the actuator leakage is used in the EKF-based fault detection scheme. Furthermore, no prior knowledge about the faulty behavior of the actuator is required in the work. Finally, the EKF model takes into account the actuator stick-slip friction, which is commonly present in any hydraulic system. The proposed FDI scheme is verified through experimental studies. The experiments reported in this paper were also performed in simulations to confirm that the observations made from the experiments truly reflect the nature of the scheme. The accuracy of the simulation program had been previously verified. Only results from the experiments are shown here, since the simulation results are consistent with the experimental observations.

2 Description of Test Rig

The experimental setup is shown in Fig. 1. The system is powered by a motor-driven hydraulic pump, which offers continuous and stable high-pressure hydraulic fluid for the actuator. The actuator is a double-rod cylinder and its movement is controlled by a Moog D765 servovalve. The valve is controlled by a high-speed PC equipped with a data acquisition board and an encoder card. When operating at 20.7MPa, the ser-

servo valve can supply the actuator with hydraulic fluid at a rate of 34L/min. However, in the experiments, the actual operating pressure is set to be 13.8MPa. All control algorithms are implemented on a high-speed PC. The displacement of the actuator is obtained by a rotary optical encoder via a Metrabyte M5312 quadrature incremental encoder card. The displacement resolution is approximately 0.03mm. Other necessary system state variables are measured by transducers mounted on the hydraulic circuit and transmitted to a DAS-16. The data acquisition board that also transmits control signals to the servovalve.

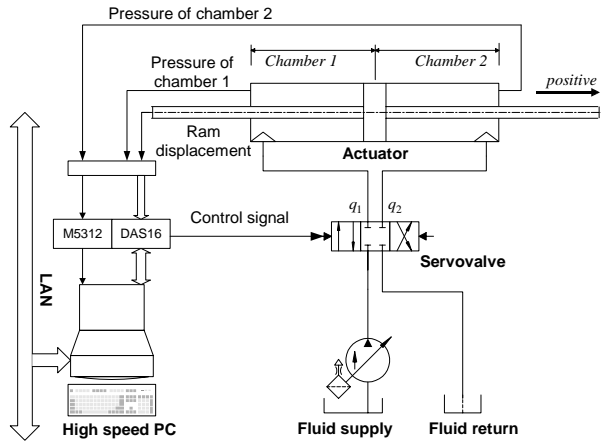


Fig. 1: Hydraulic test station on which all experiments were performed

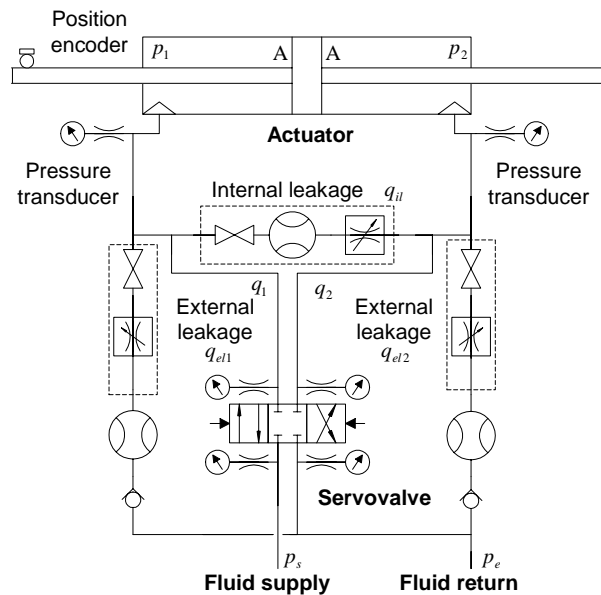


Fig. 2: Leakage faults in the actuator

Besides the main circuit, the test rig also includes a set of auxiliary circuits to simulate leakage faults of interest. Figure 2 shows the manner in which the internal leakage between the two chambers of the actuator cylinder and, the external leakage at either side of the cylinder are artificially introduced. The internal leakage is simulated by bypassing fluid across the piston. This is achieved by connecting the two chambers of the actuator and controlling the flow by an adjustable needle valve (see Fig. 2). The flow rate is measured using a positive displacement flow-meter (JVA-KL series by

AW Company) with a 7.6 L/min range and accuracy of $\pm 0.5\%$ of actual reading at 30 cst. To simulate the external leakage, a portion of the fluid flow from either side of the actuator, is bypassed to the reservoir by adjusting the appropriate flow control valves. The output of the external leakage flow control valves are measured using similar positive-displacement flow-meters. The leakages are denoted as q_{e11} and q_{e12} representing external leakages from the chambers 1 and 2, respectively, and q_{ii} representing internal (cross-port) leakage between the two chambers.

3 System Model

Understanding the dynamics of the system, under normal operation, is essential to the problem under investigation. Using a linear orifice area gradient, w , the spool displacement, x_{sp} is related to the flows out of (q_1) and into (q_2) the servovalve as shown below (Merritt, 1967):

$$\begin{cases} q_1 = C_d w x_{sp} \sqrt{\frac{2}{\rho} (p_s - p_1)} \\ q_2 = C_d w x_{sp} \sqrt{\frac{2}{\rho} (p_2 - p_e)} \end{cases} \quad x_{sp} > 0 \quad (1)$$

$$\begin{cases} q_1 = C_d w x_{sp} \sqrt{\frac{2}{\rho} (p_1 - p_e)} \\ q_2 = C_d w x_{sp} \sqrt{\frac{2}{\rho} (p_s - p_2)} \end{cases} \quad x_{sp} < 0$$

C_d is the orifice coefficient of discharge, and ρ represents the density of the hydraulic oil. Pressure variables are shown in Fig. 2. Continuity equations for the hydraulic flows between the servovalve and the actuator, in the presence of no leakage, are

$$\begin{cases} q_1 = A \dot{x} + \frac{1}{\beta} V_1(x) \dot{p}_1 \\ q_2 = A \dot{x} - \frac{1}{\beta} V_2(x) \dot{p}_2 \end{cases} \quad (2)$$

x represents the actuator displacement and β is the effective bulk modulus of the hydraulic fluid. $V_1(x)$ and $V_2(x)$ are the volumes of the fluid trapped in either chambers of the actuator and expressed by the following equations:

$$\begin{cases} V_1(x) = V_1^0 + A(x - X_{\min}) \\ V_2(x) = V_2^0 + A(X_{\max} - x) \end{cases} \quad (3)$$

where V_1^0 and V_2^0 are the volumes of hydraulic fluid trapped in the corresponding supply pipes; X_{\min} and X_{\max} are positions of the ram in its fully retracted and fully extended position, respectively. The dynamic relation between the servovalve input signal, u , and the spool displacement, x_{sp} is expressed as a typical linear

second-order system:

$$u = \frac{1}{k_{sp}\omega_n^2}\ddot{x}_{sp} + \frac{2d_m}{k_{sp}\omega_n}\dot{x}_{sp} + \frac{1}{k_{sp}}x_{sp} \quad (4)$$

where ω_n is the natural frequency, k_{sp} is the gain, and d_m is the effective damping ratio. In the absence of loading, the actuator dynamics can be represented by the following relation:

$$f_a = (P_1 - P_2)A = m\ddot{x} + F_c \quad (5)$$

In Eq. 5 m is the total inertia, and F_c denotes the actuator seal friction force. In a hydraulic actuator, due to the high fluid pressure, the seals friction is substantial and could reach up to 30% of the total driving force (Lischinsky et al, 1999). Various models have been developed to model the friction. A typical stick-slip friction model was proposed by Karnopp (1985) and was applied by some researchers (Sepehri et al, 1996). Other models, using state-space representation (Canudas-de-Wit et al, 1995) and empirical models (Kwak et al, 1999; Bonchis et al, 1999) were also developed. In this work, a series of experiments were performed on the test rig to determine the friction characteristic for the actuator under investigation. Figure 3 shows the experimental plot of steady-state (zero-acceleration) actuator force, representing F_c , at each velocity. The following improved Karnopp model (Laval et al, 1996) was found suitable to represent this plot:

$$\begin{cases} F_c = [f_{st} - (f_{st} - f_{sl})(1 - e^{-\frac{|\dot{x}|}{a}})]\frac{\dot{x}}{|\dot{x}|} + d\dot{x} & \dot{x} \neq 0 \\ F_c = f_a & f_a < f_{st} \quad \& \quad \dot{x} = 0 \\ F_c = f_{st} & f_a \geq f_{st} \quad \& \quad \dot{x} = 0 \end{cases} \quad (6)$$

f_{st} and f_{sl} represent static (stick) and slip frictions, respectively. Factor a is the constant that decides the decay ratio of the slip friction. d is the combined coefficient of modeled damping and viscous friction forces. Note that Eq. 6 also includes a model of the stick friction that includes Stribeck effects.

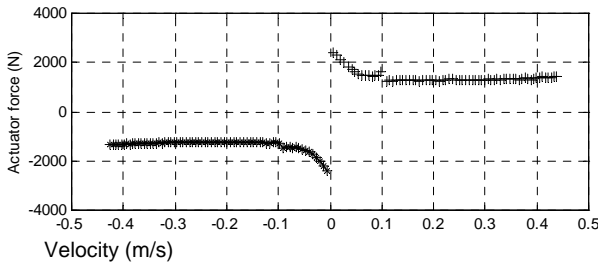


Fig. 3: Measured steady-state actuator force versus velocity

Discretizing Eq. 1 to 6, using forward difference method, and defining state vector $\mathbf{x}_k = [x_1(k), x_2(k), x_3(k), x_4(k), x_5(k), x_6(k)]^T =$

$$[x_{sp}, p_1, p_2, x, \dot{x}, \dot{x}_{sp}]^T$$

the following nonlinear discrete state-space model of the hydraulic system is obtained:

$$\begin{cases} x_1(k+1) = Tx_6(k) + x_1(k) \\ x_2(k+1) = \begin{cases} \frac{T\beta}{V_1(x_4(k))} [C_d wx_1(k) \sqrt{\frac{2}{\rho}(p_s - x_2(k))}] - Ax_5(k) + x_2(k) & x_1(k) > 0 \\ \frac{T\beta}{V_1(x_4(k))} [C_d wx_1(k) \sqrt{\frac{2}{\rho}(x_2(k) - p_e)}] - Ax_5(k) + x_2(k) & x_1(k) \leq 0 \end{cases} \\ x_3(k+1) = \begin{cases} \frac{T\beta}{V_2(x_4(k))} [-C_d wx_1(k) \sqrt{\frac{2}{\rho}(x_3(k) - p_e)}] + Ax_5(k) + x_3(k) & x_1(k) > 0 \\ \frac{T\beta}{V_2(x_4(k))} [-C_d wx_1(k) \sqrt{\frac{2}{\rho}(p_s - x_3(k))}] + Ax_5(k) + x_3(k) & x_1(k) \leq 0 \end{cases} \\ x_4(k+1) = Tx_5(k) + x_4(k) \\ x_5(k+1) = \frac{T}{m} [Ax_2(k) - Ax_3(k) - F_c(k)] + x_5(k) \\ x_6(k+1) = T[-2d_m\omega_n x_6(k) - \omega_n^2 x(k) + k_{sp}\omega_n^2 u(k+1)] + x_6(k) \end{cases} \quad (7)$$

where

$$\begin{cases} F_c(k) = [f_{st} - (f_{st} - f_{sl})(1 - e^{-\frac{|x_5(k)|}{a}})]\text{sgn}(x_5(k)) + dx_5(k) & |x_5(k)| > v_o \\ F_c(k) = f_a & f_a < f_{st} \quad \& \quad |x_5(k)| \leq v_o \\ F_c(k) = f_{st} & f_a \geq f_{st} \quad \& \quad |x_5(k)| \leq v_o \end{cases} \quad (8)$$

T represents the sampling time. v_o denotes the break away velocity, which is set to avoid numerical problems. It is set to 0.001m/s.

4 EKF Fault Detector

Extended Kalman filter and derivation of its equations can be found in many literature including references by Jazwinski (1970) and, Welch and Bishop (2001). Here, only the final equations are provided. Given the following nonlinear system,

$$\begin{cases} \mathbf{x}_k = \mathbf{f}(\mathbf{x}_{k-1}, \mathbf{u}_k, \mathbf{w}_{k-1}) \\ \mathbf{z}_k = \mathbf{h}(\mathbf{x}_k, \mathbf{v}_k) \end{cases} \quad (9)$$

where $\mathbf{f}(\cdot)$ and $\mathbf{h}(\cdot)$ are nonlinear functions describing the system state vector, \mathbf{x}_k , and the measurement vector, \mathbf{z}_k . \mathbf{u}_k is the input vector of dimension r . \mathbf{w}_k and \mathbf{v}_k , are the process and measurement noise vectors, respectively. The EKF is then grouped into two stages:

Stage one: time update equations (prediction):

$$\begin{cases} \hat{\mathbf{x}}_k^- = \mathbf{f}(\hat{\mathbf{x}}_{k-1}^+, \mathbf{u}_k, \mathbf{0}) \\ \mathbf{P}_k^- = \mathbf{A}_k \mathbf{P}_{k-1}^+ \mathbf{A}_k^T + \mathbf{W}_k \mathbf{Q}_{k-1} \mathbf{W}_k^T \end{cases} \quad (10)$$

Stage two: measurement update equations (correction):

$$\begin{cases} \mathbf{K}_k = \mathbf{P}_k^- \mathbf{H}_k^T (\mathbf{H}_k \mathbf{P}_k^- \mathbf{H}_k^T + \mathbf{V}_k \mathbf{R}_k \mathbf{V}_k^T)^{-1} \\ \hat{\mathbf{x}}_k^+ = \hat{\mathbf{x}}_k^- + \mathbf{K}_k (\mathbf{z}_k - \mathbf{h}(\hat{\mathbf{x}}_k^-, \mathbf{0})) \\ \mathbf{P}_k^+ = (\mathbf{I} - \mathbf{K}_k \mathbf{H}_k) \mathbf{P}_k^- \end{cases} \quad (11)$$

$\hat{\mathbf{x}}_k^-$ and $\hat{\mathbf{x}}_k^+$ are the *a priori* and the *a posteriori* estimates of the system states, respectively. \mathbf{K}_k is known as the Kalman gain. \mathbf{P}_k , \mathbf{Q}_k and \mathbf{R}_k are the covariance matrices related to the state vector, \mathbf{x}_k , process noise vector, \mathbf{w}_k , and measurement noise vector, \mathbf{v}_k , respectively. \mathbf{A}_k , \mathbf{H}_k , \mathbf{W}_k , \mathbf{V}_k are the Jacobian matrices, elements of which are updated at each sampling time according to the following equations:

$$\begin{aligned}
 \mathbf{A}_{k[i,j]} &= \left. \frac{\partial f_{[i]}}{\partial x_{[j]}} \right|_{(\hat{\mathbf{x}}_{k-1}^+, \mathbf{u}_k, 0)}, & \mathbf{H}_{k[i,j]} &= \left. \frac{\partial h_{[i]}}{\partial x_{[j]}} \right|_{(\hat{\mathbf{x}}_k^-, 0)}, \\
 \mathbf{W}_{k[i,j]} &= \left. \frac{\partial f_{[i]}}{\partial w_{[j]}} \right|_{(\hat{\mathbf{x}}_{k-1}^+, \mathbf{u}_k, 0)}, & \mathbf{V}_{k[i,j]} &= \left. \frac{\partial h_{[i]}}{\partial v_{[j]}} \right|_{(\hat{\mathbf{x}}_k^-, 0)}
 \end{aligned} \quad (12)$$

EKF generates a sequence of estimated state vector, $\hat{\mathbf{x}}_k$, given the measurements, \mathbf{z}_k , at each sampling time. Selected elements of the estimated state vector are then compared with the corresponding measurements to compute the state estimation error, \mathbf{e}_k . Under the normal operating condition, the state estimates of the EKF closely converge to the system states at each sampling time; thus, the residual errors, \mathbf{e}_k , stay at relatively low level, reflecting only the estimation errors and/or modelling uncertainties. However, when a fault occurs, one or more of the system parameters changes (i.e., the characteristics of the system change). Theoretically, discrepancy lies between the faulty system model and the EKF model that is designed based on the healthy system. Due to this discrepancy, the estimation of the EKF on a specific system state or states diverges from the actual state trajectory. By tracing the variation of residual errors, faults can be detected. Meanwhile, by observing the patterns of the change in the residual errors, faults can be identified.

Figure 4 shows the configuration of the proposed system. The measurements of ram displacement, x , and the two actuator chamber pressures, p_1 and p_2 , are used along with the control signal, in the EKF. By observing the variation of the moving average of the residual errors, pertaining to the chamber pressures only, leakage fault types are identified. Note that although the actuator displacement measurement was not used to determine the level and type of leakage, its use in the EKF scheme was necessary to prevent impaired estimation when no faults were present.

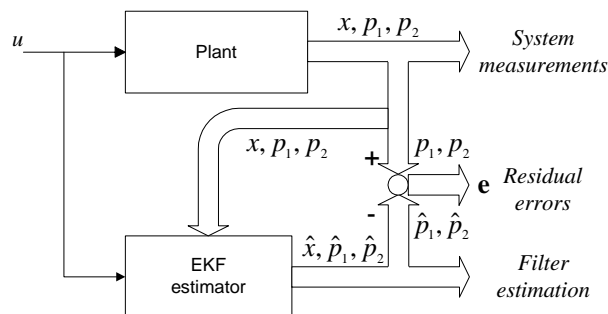


Fig. 4: Leakage fault identification scheme

A few comments about the calculation of Jacobian and covariance matrices are presented in the ensuing discussion. With reference to Fig. 4 and Eq. 9, $\mathbf{z}_k = [x(k), p_1(k), p_2(k)]^T$; thus,

$$\mathbf{H}_k = \begin{bmatrix} 0 & 0 & 0 & 1 & 0 & 0 \\ 0 & 1 & 0 & 0 & 0 & 0 \\ 0 & 0 & 1 & 0 & 0 & 0 \end{bmatrix} \quad (13)$$

The elements of matrix \mathbf{A}_k , in Eq. 12, are obtained from Eq. 7 and 8. For example, the fifth row of matrix \mathbf{A}_k that represents the dynamics of the actuator with friction, is obtained as follows:

$$\begin{aligned}
 \mathbf{A}_{k[5]} &= \frac{\partial f_{[5]}}{\partial \mathbf{x}} = \\
 &= \begin{cases} \left[0, \frac{TA}{m}, \frac{TA}{m}, 0, 1 - \left(-\frac{(f_{st} - f_{sl})}{a} e^{-\frac{|x_5(k)|}{a}} + d \right), 0 \right] & |x_5(k)| > v_0 \\ |x_5(k)| > v_0 \\ [0, 0, 0, 0, 1, 0] & f_a < f_{st} \ \& \ |x_5(k)| \leq v_0 \\ \left[0, \frac{TA}{m}, \frac{TA}{m}, 0, 1, 0 \right] & f_a \geq f_{st} \ \& \ |x_5(k)| \leq v_0 \end{cases} \quad (14)
 \end{aligned}$$

covariance matrices \mathbf{Q}_k and \mathbf{R}_k are considered constants assuming noises are stationary, white and Gaussian. Further, it is assumed that the noise characteristics of different system state variables are independent of each other. Thus, both \mathbf{Q}_k and \mathbf{R}_k are diagonal, and the values of their elements should be estimated prior to the experiment. Finally, it can be drawn from the assumptions of the noise vectors that the Jacobian matrices of \mathbf{W}_k and \mathbf{V}_k are unity matrices.

5 Experimental results

Experiments were carried out on the test rig shown in Fig. 1, to evaluate the leakage fault identification strategy described in Section 4. The parameters of the experimental test rig, used in the EKF model, are summarized in Table 1. Values of these parameters were obtained directly from manufacturer's data, by careful experimental measurement, and through comparisons between the results of nonlinear simulations and experimental trials. For example, the values of slip friction (f_{sl}) and stick friction (f_{st}) were obtained from the experimentally obtained graph of Fig. 3. The value of

Table 1: Hydraulic test rig parameters

A (m ²)	633×10^{-6}	k_{sp} (m/V)	40.6×10^{-6}	P_s (Pa)	13.79×10^6
m (kg)	10.0	ω_n (Hz)	100	β (Pa)	689×10^6
X_{min} (m)	0.0	d_m	0.7	ρ (kg/m ³)	847
X_{max} (m)	0.606	V_1^0, V_2^0 (m ³)	21.4×10^{-6}	C_v	0.6
d (Ns/m)	350	P_e (Pa)	0.0	w (m ² /m)	20.75×10^{-3}
f_{sl} (N)	1100	f_{st} (N)	2200	a (m/s)	0.6

β , reported in Table 1, has been taken from Merritt (1967). Alternatively, estimation of critical parameters of the system can be made using the EKF (see Chinniah et al, 2003).

The initial state vector, $\hat{\mathbf{x}}_0^+$, and the covariance matrix, \mathbf{P}_0^+ , can be accordingly set to the expected values (Haykin, 2001). In practice, \mathbf{P}_0^+ can be set to a sufficiently positive-definite matrix that is diagonally salient. Here, \mathbf{P}_0^+ was set to be a diagonal matrix with $\mathbf{P}_{0[i,i]}^+ = 10^4$. The values for the state estimates were initially set to zeros except for the line pressures which were set to half of the pump pressure, i.e., $\hat{\mathbf{x}}_0^+ = [0, 6.8 \times 10^6, 6.8 \times 10^6, 0, 0, 0]^T$.

In order to produce a good convergence rate, the determination of covariance matrices, \mathbf{Q}_k and \mathbf{R}_k , was based on a combination system noise analysis, consideration of modelling uncertainties and a comparison between the simulation and experimental results. Having a precise model of the servovalve, the estimation of the spool displacement was very close to the actual measurement. Therefore the influence of the process noise in the spool displacement measurement can be almost neglected, which is finally determined as 10^{-10} m. Similarly the uncertainty of the chamber pressures was estimated by observing the error between the simulation results and the actual experiments given the same inputs for the servovalve. The matrix \mathbf{Q} is given as $\mathbf{Q} = \text{diag}[10^{-10} \ 10^2 \ 10^2 \ 10^{-3} \ 10^{-2} \ 10^{-10}]$. The measurement noise variances were determined as 10^{-2} m for the ram displacement, and 10^3 Pa for the chamber pressures. Thus, the matrix \mathbf{R} is given as $\mathbf{R} = \text{diag}[10^{-2} \ 10^3 \ 10^3]$.

For all the tests reported here, a sinusoidal input signal with a frequency of 0.5Hz and amplitude of 3V, was applied for 40s to test the scheme. The external leakage on either side of the actuator cylinder as well as the internal leakage between the two cylinder chambers were introduced by opening the bleed valves mounted on corresponding bypasses (as was described earlier). For every test, the system started under normal operating condition. At approximately 18 seconds into the operation, various leakage faults were introduced by manually adjusting the bleed valves. For each leakage type, two levels of leakages, low and high, were tested. The sampling time was $T=0.001$ s.

Figures 5 to 8 show the results of the first test in

which an external leakage, q_{el1} , was introduced in chamber 1. The plot of the leakage is given in Fig. 5. As is seen, due to the dynamics of the system, q_{el1} is not constant. Thus, in order to quantify the leakage level, for comparison purposes only, a coefficient of leakage is defined here. Thompson et al (1999) suggested the piston seal leakage can be modeled as a turbulent orifice flow. Merritt (1967) suggested a linear relation between the internal and the external leakages, and the corresponding pressure differentials. Here, we use the latter definition. Thus, the external leakage coefficient at chamber 1, k_{el1} , is defined as

$$k_{el1} = \frac{q_{el1}}{(p_1 - p_e)} \quad (15)$$

From Fig. 5, the mean value of leakage coefficient is found to be $k_{el1} = 1.589 \times 10^{-12}$ m³/s·Pa with the standard deviation of $\sigma_{el1} = 3.787 \times 10^{-13}$ m³/s·Pa. Figures 6 to 8 compare the measurements with those estimated by extended Kalman filter. The average of the errors over a moving window of data is used for detecting faults. The moving average of the errors, e_a , is calcu-

lated from $e_a = \frac{\sum_{i=k-n}^k |e_i|}{n}$, where the size of the data, n ,

for calculating the moving average was 4000 (sampled at 1000Hz) in this work. From Fig. 6, it is seen that the actuator started to drift once the leakage fault was introduced. This is expected due to the leakage at chamber 1, which reduced the power to equally push the piston to either side. However, the error between the displacement measurement and the one from the Kalman filter remained the same (and so did the moving average) even after the introduction of the external leakage fault. Thus, little information can be obtained by observing the displacement plots in the presence of external leakage fault and given the scheme proposed here. However, with reference to Fig. 7, it can be seen that the residual error of pressure, p_1 , is small during the no-fault period; but once the fault is introduced in the system, the estimated pressure diverges from the actual measurement. The subplot for the moving average of the residual error between the measured and the estimated chamber 1 pressure, shows that it increased an average of 1.251×10^5 Pa for an average leakage of 0.583L/min. Figure 8 shows that moving average error of chamber 2 pressure did not change even after the

leakage was introduced.

Due to the symmetric structure of the actuator cylinder and the rod, the performance of the EKF in the presence of external leakage fault in chamber 2 is similar to that of chamber 1. Figure 9 and 10 show the experimental results related to the external leakage fault introduced in chamber 2. Figure 9 shows plots of the leakage fault and the corresponding displacement response. The mean coefficient of external leakage in chamber 2, k_{e12} , was estimated, following a similar relation as in (15), as $k_{e12} = 1.676 \times 10^{-12} \text{ m}^3/\text{s}\cdot\text{Pa}$ with standard variance $\sigma_{e12} = 3.457 \times 10^{-13} \text{ m}^3/\text{s}\cdot\text{Pa}$. From Fig. 10, it is seen that the moving average of the residual error for the pressure at chamber 2, changed from an average of $0.903 \times 10^5 \text{ Pa}$ to approximately $2.2 \times 10^5 \text{ Pa}$ within a short period of time. However the moving average of the residual error at chamber 1 did not change significantly after the fault had occurred.

The third test was to observe the response of the EKF-based fault detector to the internal leakage. The internal leakage flows from the higher-pressure chamber to the lower pressure chamber of the actuator. This leakage was simulated by adjusting the needle valve mounted on the bypass that connected the two chambers of the actuator as was described earlier. Figure 11 shows plots of the displacement and the internal leakage given a sinusoidal input voltage similar to the previous tests. The average leakage coefficient was determined to be $k_{i1} = 8.854 \times 10^{-12} \text{ m}^3/\text{s}\cdot\text{Pa}$ with the standard deviation of $\sigma_{i1} = 3.242 \times 10^{-2} \text{ m}^3/\text{s}\cdot\text{Pa}$. Exploring the experimental results shown in Fig. 12, it is observed that the moving average of the residual errors of both chamber pressures increased ($0.560 \times 10^5 \text{ Pa}$ and $0.902 \times 10^5 \text{ Pa}$ for chambers 1 and 2, respectively) with the introduction of an internal leakage of $\approx 0.825 \text{ L}/\text{min}$.

The above typical tests clearly show that by observing the residual error of the chamber pressures one could identify the occurrence of various leakage faults. The increase of the residual error of one of the chambers only, indicates the occurrence of the external leakage in that chamber. However, when the cross-port leakage occurs, the residual errors for both the chamber pressures increase.

The last test was to investigate whether different levels of leakage faults can be distinguished. Figure 13, 14 and 15 show the results of implementing three types of leakage faults. Table 2 shows the leakage fault levels

applied. The variation of the residual errors related to the change of leakage flows is also shown. This set of experiments demonstrates the level of sensitivity of the EKF-based fault detector scheme introduced in this paper. For example with reference to Fig. 13, it is seen that with the increase of the level of external leakage at chamber 1, the moving average of the residual error of the An and Sepehri (2003) developed an EKF-based scheme capable of detecting the incorrect supply pressure fault and experimentally verified that the scheme could effectively detect a pressure change of less than 10% of the nominal value. Chinniah et al (2003) showed that the bulk modulus and the viscous damping coefficient of a hydrostatic actuation system could be correctly estimated, in sequence, using EKF. From the above papers, it is noted that a general approach for fault detection and isolation in nonlinear fluid power systems is complicated to develop. Also, the actuator leakage fault detection has not yet received enough attention. Karpenko and Sepehri (2004) developed a fault tolerant control scheme for a hydraulic servo-positioning system with a faulty actuator piston seal that causes internal leakage. They showed that implementing a fault tolerant control scheme allows the closed-loop performance to be maintained despite the internal leakage until the system can be safely shut down and the faulty seal replaced. Although its importance was discussed, the paper did not consider the identification of level and type of leakage.

In this paper, we develop and experimentally evaluate, for the first time to our knowledge, a scheme that employs EKF to identify various leakage type faults in an electrohydraulic actuator. External leakage from either side of the actuator, and cross-port leakage between the two chambers are considered. corresponding chamber pressure increases. Figures 14 and 15 illustrate consistent observations with respect to the leakage at chamber 2 as well as internal leakage, respectively. The experiments also revealed that in average, residual pressure errors less than $\approx 1.05 \times 10^5 \text{ Pa}$ must be considered normal.

Note that although the actuator displacement measurements is not employed to decide on the type and level of leakage, in this study, its use in the EKF scheme was necessary to prevent impaired estimation in the present of no fault.

Table 2: Leakage faults parameters in open loop mode

	External leakage chamber 1		External leakage chamber 2		Internal leakage	
	Low	High	Low	High	Low	High
Leakage level						
Mean value of the leakage coefficient ($\text{m}^3/\text{s}\cdot\text{Pa}$) $\times 10^{-12}$	1.589	3.334	1.676	4.257	8.854	11.503
Standard deviation (m^3/s) $\times 10^{-13}$	3.787	8.419	3.457	10.760	32.410	41.339
Average change in residual errors						
Chamber 1 pressure (Pa) $\times 10^5$	1.251	2.519	0.082	0.357	0.560	1.091
Chamber 2 pressure (Pa) $\times 10^5$	0.121	0.345	1.323	2.949	0.902	1.449

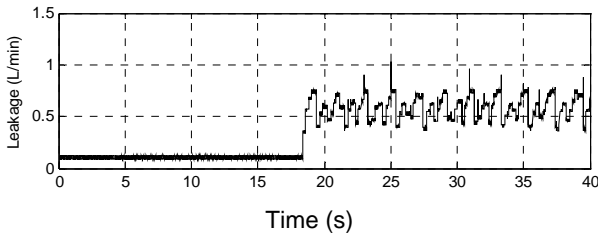


Fig. 5: External leakage fault introduced at $t \approx 18s$ to chamber 1

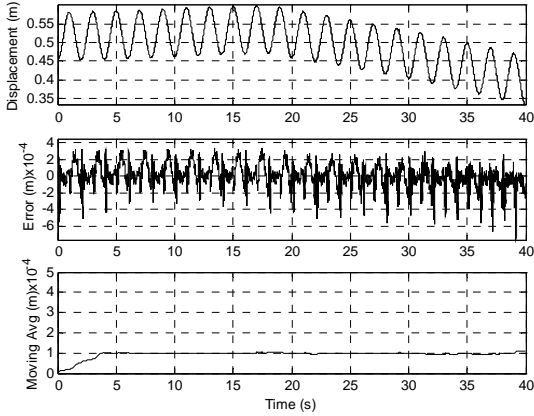


Fig. 6: Ram displacement, residual error, and the moving average of the error in the presence of external leakage fault at chamber 1 shown in Fig. 5

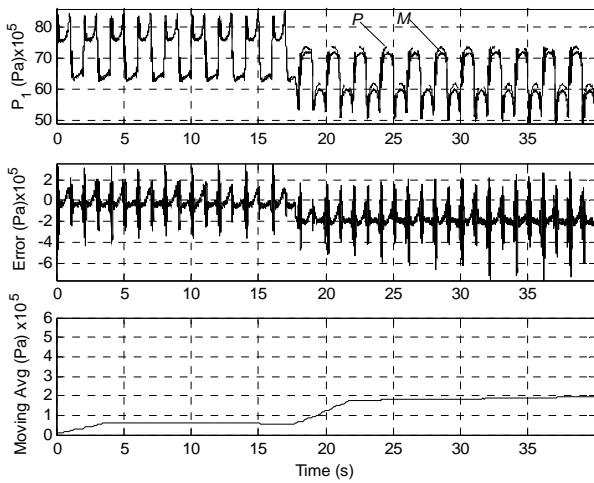


Fig. 7: Measured (M) and predicted (P) chamber 1 pressure, P_1 , residual and moving average errors in the presence of external leakage fault at chamber 1 shown in Fig. 5

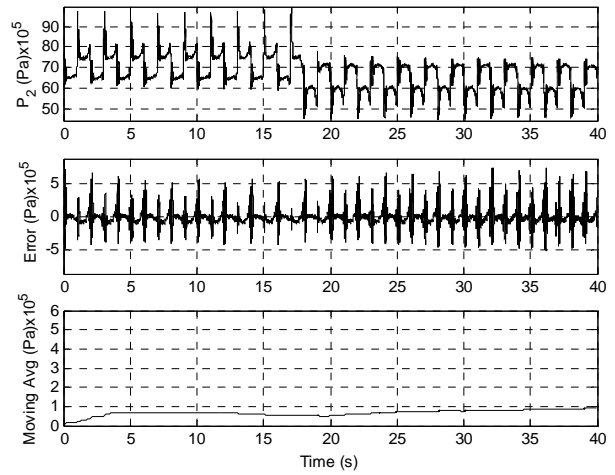


Fig. 8: Measured and predicted chamber 2 pressure, P_2 , residual and moving average errors in the presence of external leakage fault at chamber 1 shown in Fig. 5

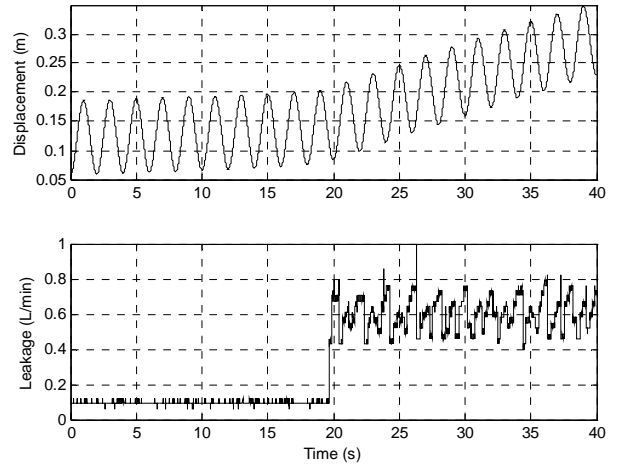


Fig. 9: Ram displacement and external leakage introduced at $t \approx 18s$ to chamber 2

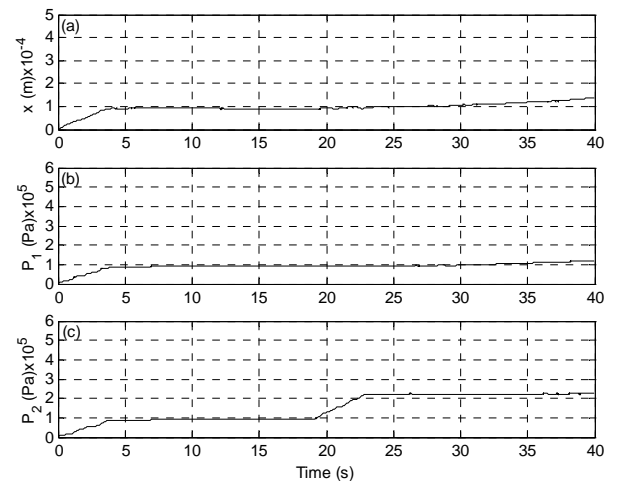


Fig. 10: Moving average of residual errors given external leakage shown in Fig. 9: (a) displacement, x ; (b) chamber 1 pressure, P_1 ; (c) chamber 2 pressure, P_2

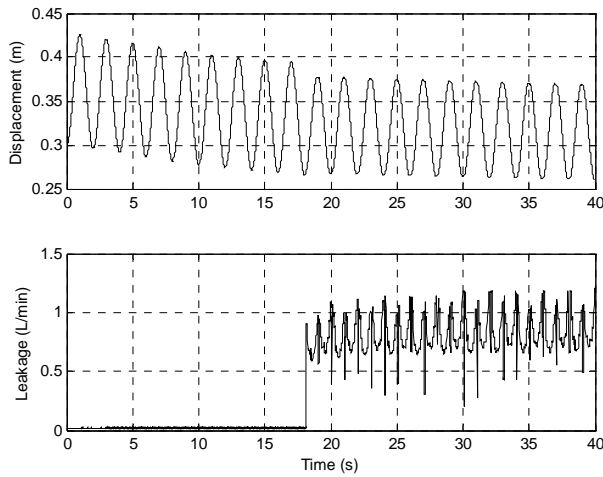


Fig. 11: Ram displacement and internal leakage, introduced at $t \approx 18s$, between the two chambers

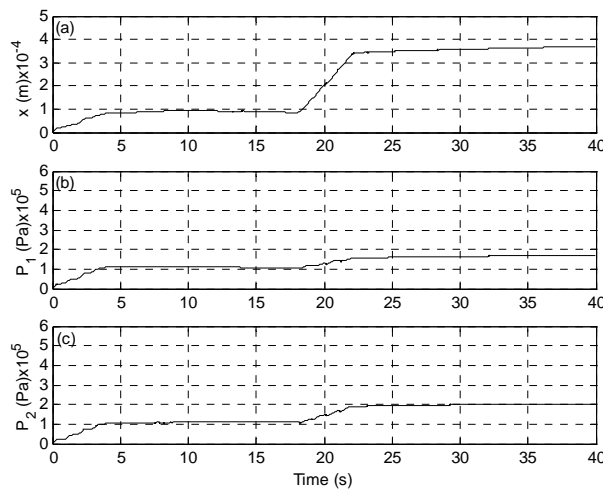


Fig. 12: Moving average of residual errors given internal leakage fault as shown in Fig. 11: (a) displacement, x ; (b) chamber 1 pressure, P_1 ; (c) chamber 2 pressure, P_2

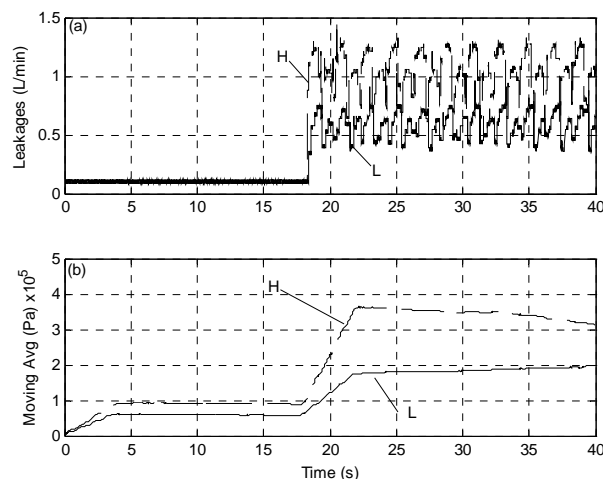


Fig. 13: Response of leakage fault detector to different fault levels: (a) external leakage in chamber 1; (b) moving average of residual pressure errors in chamber 1 (dashed line - High leakage, solid line - Low leakage)

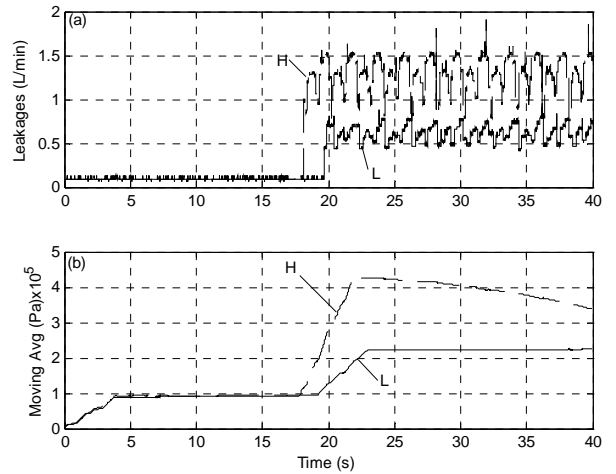


Fig. 14: Response of leakage fault detector to different fault levels: (a) external leakage in chamber 2; (b) moving average of residual pressure errors in chamber 2 (dashed line - High leakage, solid line - Low leakage)

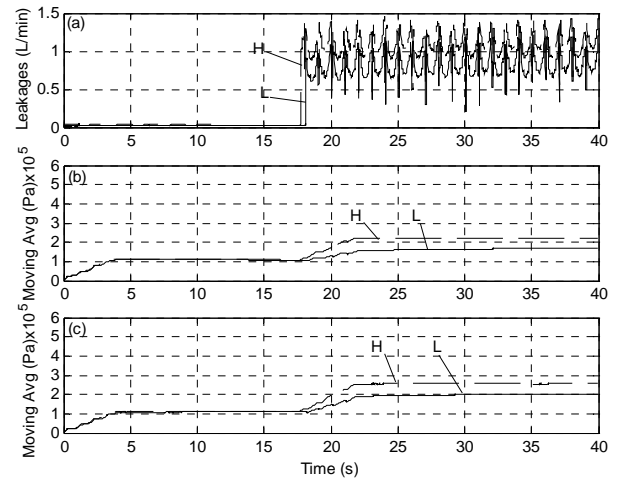


Fig. 15: Response of the leakage fault detector to different fault levels: (a) internal leakages; (b) moving average of residual pressure errors in chamber 1; (c) moving average of residual pressure errors in chamber 2 (dashed line - High leakage, solid line - Low leakage)

6 Conclusions

This paper documented, for the first time*, the diagnosis of experimental actuator leakage faults using extended Kalman filter in a hydraulically-powered actuator. A fault-free model of the nonlinear hydraulic functions coupled with a comprehensive model of the actuator dry friction, that includes stick-slip friction and Stribeck effect, was first derived. With only three low-cost measurements, i.e., actuator displacement and line pressures, the constructed EKF-based fault detector

* Remark of Editor-in-Chief: This method has been already verified in experiment, e.g. Abbas Kazemi-Moghaddam. 1998. Early fault detection and diagnosis of an electrohydraulic linear drive system. Thesis (PhD). Technical University of Darmstadt. Germany. Published in german language: "Fehlerfrüherkennung und -diagnose eines elektrohydraulischen Linearantriebssystems".

was experimentally shown to successfully identify external and internal leakage faults in the actuator. It was shown that according to the residual errors obtained by monitoring the chamber pressures only, different patterns can be obtained, which can be used to detect leakage faults at the early stage. Particularly, it was observed that the magnitude of the change of the residual errors, caused by the leakage faults, increase proportionally with the increase of fault levels. This is significant since it allows the progress of the leakage flows to be monitored. In its present form, the approach described in this paper can be used towards manual condition monitoring of hydraulic systems with respect to actuator's leakage faults. Future work would involve further examination of the sensitivity of the scheme to leakage faults as well as robustness in the presence of unknown loading conditions. Development of an on-line scheme to continuously detect the health of the system is another challenging future project.

References

- An, L., Sepehri, N.** 2003. Hydraulic actuator circuit fault detection using extended Kalman filter. *Proceedings of American Control Conference*, Vol. 5, pp. 4261 – 4266.
- Bonchis, A., Corke, P.I., Rye, D.C.** 1999. A pressure-based, velocity independent, friction model for asymmetric hydraulic cylinders. *Proceedings of the IEEE International Conference on Robotics and Automation* Vol. 3, pp. 1746 – 1751.
- Canudas-de-Wit C., Olsson, H., Astrom, K. J., Lischinsky, P.** 1995. A New Model for Control of Systems with Friction. *IEEE Transactions on Automatic Control*, Vol. 40, pp. 419-425.
- Chinniah Y, Burton, R. and Habibi, S.** 2003. Viscous damping coefficient and effective bulk modulus estimation in a high performance hydrostatic system using extended Kalman filter. *International Journal of Fluid Power*, Vol. 4, pp. 27-34.
- Crowther, W.J., Edge, K. A., Atkinson R.M., and woollons D.J.** 1998. Fault diagnosis of a hydraulic actuator circuit using neural networks – an output vector space classification approach. *Proc. Instn. Mech. Engrs.*, Vol. 212, pp. 57-68.
- Frank, Paul M.** 1994. On-line fault detection in uncertain nonlinear system using diagnostic observers: a survey. *International Journal of System Science*, Vol. 25, pp. 2129-2154.
- Haykin, S.** 2001. *Kalman filtering and neural networks*. John Wiley & Sons Inc.
- Isermann, R.** 1997. *Supervision, Fault-Detection and Fault-Diagnosis Methods – An Introduction*. Control Engineering. Practice, Vol. 5, pp. 639-652.
- Jazwinski, H. A.** 1970. *Stochastic processes and filtering theory*. Academic press.
- Karpenko, M., Sepehri, N.** 2004. Fault tolerant control of a servohydraulic positioning system with cross-port leakage. *IEEE Transactions on Control Systems Technology*, in press.
- Kwak, Byung-Jae, Yagle, A.E., Levitt, J.A.** 1999. Nonlinear system identification of hydraulic actuator friction dynamics using a finite-state memory model. *Proceedings IEEE International Conference on Acoustics, Speech, and Signal Processing*, Vol. 3, pp. 1309-1312.
- Khan, H., Abou, S. and Sepehri, N.** 2002. Fault detection in electro-hydraulic servo-positioning systems using sequential test of Wald. *Proceedings of Canadian conference on electrical & Computer Engineering*, pp. 1628-1633, 2002.
- Laval, L., M'Sirdi, N.K., Cadiou, J.-C.** 1996. H_{∞} -force control of a hydraulic servo-actuator with environmental uncertainties. *Proceedings of the IEEE International Conference on Robotics and Automation*, Vol. 2, pp. 1566 – 1571.
- Lischinsky, P., Canudas-de-Wit, C., Morel, G.** 1999. Friction compensation for an industrial hydraulic robot, *IEEE Control Systems Magazine*, Vol. 19, pp. 25-32.
- Merritt, H. E.**, 1967. *Hydraulic control systems*. Wiley Inc.
- Preston, G.J., Shields, D.N., Daley, S.** 1996. Application Of A Robust Nonlinear Fault Detection Observer To A Hydraulic System. *UKACC International Conference on Control*, Vol. 2, pp. 1484-1489.
- Sepehri, N., Sassani, F., Lawrence, P. D.** 1996. Ghasempour A., Simulation and Experimental Studies of Gear Backlash and Stick-slip Friction in hydraulic Excavator Swing Motion. *Journal of Dynamic Systems, Measurement, and Control*, Vol. 118, pp. 463-467.
- Skormin, V.A., Apone, J., Dunphy, J.J.** 1994. On-line diagnostics of a self-contained flight actuator. *IEEE Transactions on Aerospace and Electronic Systems*, Vol. 30, pp.186-196.
- Skormin, V.A., Apone, J.** 1995. On-line diagnostics of a variable displacement pump of a flight actuation system. *Proceedings of the IEEE National Aerospace and Electronics Conference*, Vol. 1, pp. 503-510.
- Song, R., Sepehri, N.** 2002 Fault detection and isolation in fluid power systems using a parametric estimation method. *IEEE CCECE Canadian Conference on Electrical and Computer Engineering*, Vol. 1, pp. 144-149.
- Tan, Hong-Zhou, Sepehri, N.** 2002. Parametric fault diagnosis for electrohydraulic cylinder drive units, Industrial Electronics. *IEEE Transactions on Industrial Electronics*, Vol. 49, pp. 96-106.
- Thompson, D.F., Pruyn, J.S., Shukla, A.** 1999. Feedback design for robust tracking and robust stiffness

in flight control actuators using a modified QFT technique. *International Journal of Control*, Vol. 72, pp. 1480-1497.

Welch, G., Bishop, G. 2001. *An introduction to the Kalman Filter*, UNC-Chapel Hill, 2001.

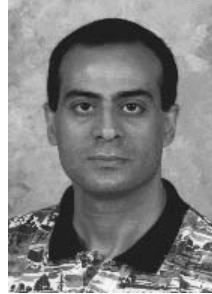
Yu, Dingli, Shields, D.N., Mahtani, J.L. 1994. Fault detection for bilinear systems with application to a hydraulic system. *Proceedings of the Third IEEE Conference on Control Applications*, Vol. 2, pp. 1379-1384.

Zavarehi, M. K., Lawrence, P. D., Sassani, F. 1999. Nonlinear modelling and validation of solenoid-controlled pilot-operated servovalves. *IEEE/ASME Transactions on Mechatronics*, Vol. 4, pp. 324-334.



Liang An

received B. Sc. in Automation Engineering from the Zhengzhou Institute of Technology in 1993, and an M. Sc. in Control Engineering from the Beijing University of Chemical Technology in 1999. His research interests include robotics, system estimation, and control engineering. He is currently a Ph.D. candidate at the University of Manitoba.



Nariman Sepehri

is a professor with the Department of Mechanical and Manufacturing Engineering, at the University of Manitoba. He received M.Sc. and Ph.D. both from the University of British Columbia. His areas of interest include telerobotics applied to heavy-duty hydraulic machines and fluid power control and diagnosis systems.